Powder Technology 379 (2021) 428–437

Contents lists available at ScienceDirect

Powder Technology

journal homepage: www.elsevier.com/locate/powtec

Irreversible expansion of silica-gel beads and quantification of pore structure made by silica-gel bead infiltration method

Hua Li [a,b], Yan Gao [a,d,*], Yuyuan Zhao [c]

[a] School of Materials Science and Engineering, South China University of Technology, Guangzhou 510640, PR China
[b] School of Advanced Manufacturing Technology, Guangdong Mechanical & Electrical Polytechnic, Guangzhou 510515, PR China
[c] School of Engineering, Universtiy of Liverpool, Liverpool L69 3GH, United Kingdom
[d] Guangdong Provincial Key Laboratory of Advanced Energy Storage Materials, PR China

ARTICLE INFO

Article history:
Received 20 July 2020
Received in revised form 11 October 2020
Accepted 29 October 2020
Available online 02 November 2020

Keywords:
Cu-based shape memory foams
Silica-gel beads expansion
Pore structure calculation
Infiltration foaming method

ABSTRACT

The irreversible expansion of silica-gel beads upon heating makes the silica-gel bead infiltration method a novel method for manufacturing Cu-based shape-memory foams with adjustable pore structures. The mechanism of silica-gel bead expansion, however, is not clear, making control and prediction of the pore structure difficult. This paper investigated the expansion mechanism of silica-gel beads by measuring expansion ratios and observing microstructural changes during heating. The irreversible and non-uniform expansion was caused by high-pressure steam generated from water confined in the nano-pores of the silica-gel beads. A geometrical model was developed to calculate the pore structures and the influences of expansion ratio and bead indentation on pore structure were discussed. The calculated values for pore size, porosity and specific surface area agreed well with the experimental results with small relative errors of 0.1% ~ 5.2%. The model will help to control the pore structure manufactured by the silica-gel bead infiltration method more precisely.

1. Introduction

Cu-based shape memory foams (SMFs) have attracted interests both in academic studies and industrial applications for their high damping property and high super-elasticity derived from the shape memory alloy (SMA) matrix [1–4]. Coupled with the intrinsic properties of metal foams [5], such as lightweight, high damping, energy absorbing capacity and high specific strength, Cu-based SMFs are promising materials for applications in sectors such as civil engineering and automobile industry.

The performance of Cu-based SMFs is affected by pore structure and pore morphology. Non-uniform foam morphology and irregular pore shape can cause high stress concentration and undesirable effect on the mechanical and functional properties of SMFs [6,7]. Many foaming methods, such as sintering-dissolution [8], sintering-evaporation [7] and melt infiltration [9], use salt space holders such as NaCl and $NaAlO_2$, which could not guarantee a uniform and regular spherical pore structure. Spherical silica-gel beads were first used as space holders by Castrodeza et al [10] to manufacture Cu-based foams and nearly spherical pore morphology was obtained.

Silica-gel beads infiltration method is a novel method developed by Li et al [3,11] to manufacture Cu-based SMFs with a uniform and adjustable pore structure (porosity from 66% ~ 82%) with spherical pore morphology. It has several advantages: a) guaranteed spherical pores due to the spherical shape of the silica-gel beads; b) uniform pore morphology due to a well-bonded silica-gel beads preform created during the heating process; c) adjustable porosity from 66% to 82% by taking advantage of the expansion feature of the silica-gel beads [11]. The as-manufactured Cu-based SMFs exhibit highly improved mechanical and functional properties such as high damping and super-elastic recovery [3], because the spherical pore morphology and uniform distribution help to avoid local stress concentration. Adjustable pore structures enable adjustable functional properties of the Cu-based SMFs, because pore structure also has a significant influence on the shape memory behavior of the SMA matrix, especially for SMA foams with an oligocrystalline microstructure [2,3].

In silica-gel beads infiltration method, the silica-gel beads expand upon heating, forcing the beads to squeeze against each other. Under the constraint of the mother alloy placed above, the point contacts among the beads are deformed to create face contacts, bonding the beads together. The expansion and indentation of the beads in this process lead to a change in the volume of the silica-gel beads and thus the porosity of the foam. It was found that the higher the bead density, the more bead deformation and the higher the porosity of the resultant

* Corresponding author at: School of Materials and Engineering, South China University of Technology, Guangzhou 510640, PR China.
E-mail address: meygao@scut.edu.cn (Y. Gao).

https://doi.org/10.1016/j.powtec.2020.10.090
0032-5910/

foam [3], which can be used as an effective mechanism to adjust the porosity.

The adjustment of pore structure produced the silica-gel beads infiltration method, however, is largely achieved by trial and error up to date. Although the empirical approach is acceptable in most cases, more accurate control of targeted pore structure and foam properties requires quantification of the expansion of the silica-gel beads. The mechanism of the irreversible expansion of silica-gel beads, which is important for predicting and controlling the pore structure, is however not understood yet. A quantitative understanding of the relationship between the pore structure of the foam and the expansion behavior of the silica-gel beads is essential.

This paper investigates the mechanism of the irreversible expansion of silica-gel beads by studying the microstructural changes and expanding patterns of the beads during heating. A geometrical model is developed to calculate the pore size, porosity and specific surface area of the foam as a function of expansion ratio of the silica-gel beads. The model predictions are compared with experimental results to validate the model.

2. Experimental procedure

The silica-gel beads used in this study were a commercial desiccant made of pure amorphous SiO_2. The raw silica-gel beads were first sieved into a series of size ranges. Two bead radius ranges, 0.25–0.36 mm and 0.36–0.50 mm, were selected for the study. The two groups of silica-gel beads were subjected to a preheating treatment as shown in Fig. 1, first at 200 °C for 1 h and then at 975 °C, 980 °C or 990 °C for 2 h. The silica-gel beads after preheating were sieved again into bead radius ranges of 0.25–0.36 mm, 0.36–0.50 mm, 0.50–0.63 mm and 1.0–1.25 mm. Five types of silica-gel beads with different combinations of raw bead size and preheating treatment, #1 - #5 as shown in Table 1, were then subjected to a final heating process to simulate the thermal procedure in the melt infiltration process used in manufacturing Cu-Al-Mn foams [3], except that the silica-gel beads were allowed to expand freely without any constraint here. Specifically, they were heated at a heating rate of 5–10 °C/min to 1100 °C and, after holding for 20 min, cooled down in furnace to room temperature, as shown in Fig. 1.

The bead radius distributions of the five types of silica-gel beads were measured using the Image Pro 6.0 software. Macroscopic images of the silica-gel beads were taken by a digital camera together with a scale and 500–1000 beads for each type from the images were measured.

The bead density, ρ, and packing density, K_{sp}, of each of the five types of silica-gel beads were measured by weighing a specific amount of beads and measuring the bulk and net volumes of the beads. The beads were poured into and loosely filled up a cylinder, which was then filled with water until the beads were fully submerged. The volume of the cylinder, V_c, and the volume of the water used to fill up the beads-containing cylinder, V_w, were measured. The bulk volume of the beads, or the combined volume of the beads and the water, was the volume of the cylinder, V_c. The net volume of the beads was the difference between the bulk volume and the volume of water, $(V_c - V_w)$. The bead density was obtained by $\rho = M/(V_c - V_w)$, where M is the mass of the beads and the packing density was obtained by $K_{sp} = 1 - V_w/V_c$.

The coordination number of the loosely packed silica-gel beads, i.e. the average number of beads in contact with any particular bead, was measured by taking advantages of the expansion feature of the silica-gel beads. In order to observe the bead contact deformation more clearly, larger silica-gel beads with a radius range of 1.0–1.25 mm and a density of 0.78 g/cm^3, which would expand and deform much more than #1 ~ #5, were used. The beads were poured into a crucible, a perforated ceramic plate was placed on top of the beads, and a block of metal was placed above the ceramic plate to simulate the pressure experienced by the silica-gel beads before the melt infiltration during the manufacturing process for the Cu-Al-Mn foams [3]. The crucible was then placed in a furnace and underwent the final heating process shown in Fig. 1. During the heating process, the beads underwent constrained expansion and the contact points between the neighboring beads were indented. After cooling down, the deformed faces of all the silica-gel beads (Fig. 2) were counted. The average number of deformed faces per bead was therefore the coordination number.

The average expansion ratios of the five types of silica-gel beads during the preheating treatment and final heating procedure were estimated from the measured bead densities of the silica-gel beads before and after the heating procedures by:

$$\frac{\Delta r}{r} \approx \frac{1}{3}\left(\frac{\rho_0}{\rho_1} - 1\right) \tag{1}$$

where $\Delta r/r$ is the average preheating or final expansion ratio, and ρ_0 and ρ_1 are the average densities of the silica-gel beads before and after the heating procedure, respectively. The silica-gel beads before the preheating treatment contain large amount of confined water, which

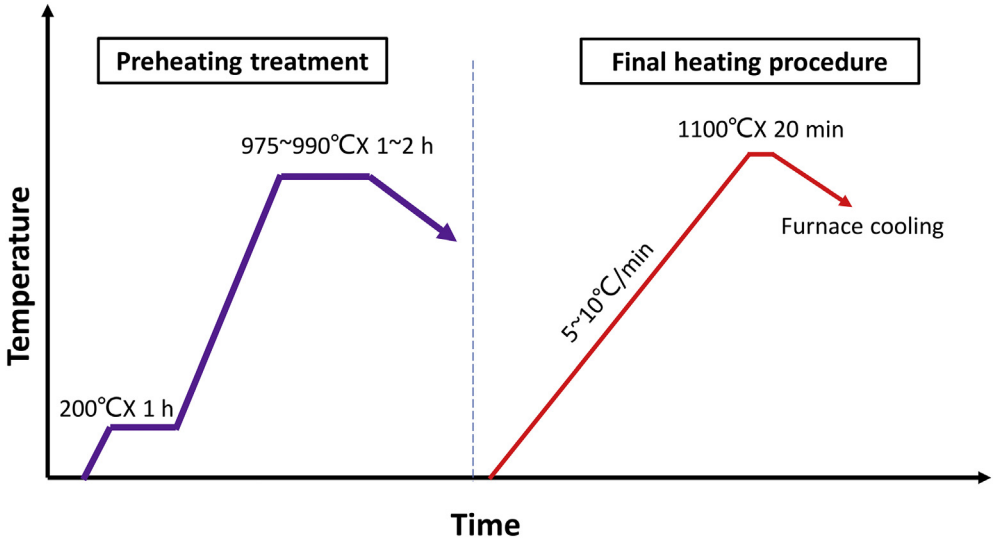

Fig. 1. Preheating treatment and final heating procedure for silica-gel beads.

Table 1
Mean bead sizes and expansion ratios after preheating and final heating processes for the five types of silica-gel beads.

Beads	Raw bead radius [mm]	Preheating process	Preheated bead density [g/cm^3]	Preheated bead radius [mm]	$\bar{r}$ [mm]	$\bar{r}_s$ [mm]	Standard difference of radius [mm]	Expansion ratio, Δr/r	
								Preheating	Final heating
#1	0.25–0.36	990 °C + 2 h	1.15	0.25–0.36	0.336	0.338	0.038	0.05	0.022
#2	0.25–0.36	990 °C + 2 h	0.74	0.36–0.50	0.444	0.446	0.040	0.26	0.024
#3	0.36–0.50	975 °C + 2 h	0.70	0.50–0.63	0.546	0.547	0.039	0.30	0.026
#4	0.25–0.36	975 °C + 2 h	0.82	0.36–0.50	0.426	0.427	0.039	0.20	0.057
#5	0.36–0.50	980 °C + 2 h	0.93	0.36–0.50	0.466	0.468	0.046	0.14	0.122

Fig. 2. Macrograph of silica-gel beads with constrained expansion after the final heating treatment.

can distort the actual density and the expansion ratio calculations. The density of the silica-gel beads before the preheating treatment (1.32 g/cm^3) was therefore estimated from the density of dense silica-gel (2.2 g/cm^3) and the porosity of the raw silica-gel beads (40%).

The cross-sectional microstructure of the silica-gel beads was observed using a Supra 40 scanning electron microscope (SEM). The silica-gel beads were inlayed in bakelite and mechanically ground and polished for cross-section observation. The samples were cleaned, dried and then gold-sprayed before observation.

3. Expansion of silica-gel beads

3.1. Mean bead radius, packing density and coordination number

The values of the volume mean radius, or average radius, $\bar{r}$, of the five types of silica-gel beads are shown in Table 1. The silica-gel beads used in this study are not uniform-sized and have a size range. The beads after expansion, either after the preheating treatment or after the final heating process, also have a size distribution. The average radius of each of the five types of silica-gel beads was determined by measuring the net volume of a powder sample and counting the number of the beads in the sample. While average radius is good for representing volume based parameters, e.g. porosity, it is normally not suitable for estimating surface related parameters such as specific surface area. Fig. 3 shows the bead radius distributions of the five types of silica-gel beads (#1 - #5). They all follow a similar log-normal distribution with a standard difference between 0.038–0.046. The surface mean radius, $\bar{r}_s$, determined using Eq. (2) [12], and the standard difference of each of the five types of beads are listed in Table 2.

$$\bar{r}_s = \sqrt{\frac{1}{n}\sum_{1}^{n} r_i^2} \tag{2}$$

Fig. 3 shows that the bead size ranges of the silica-gel beads are wider than the nominal size ranges obtained by sieves, and the average sizes also deviate from the midpoints of the nominal size ranges. This indicates that it is necessary to use experimentally measured mean bead sizes, especially for the estimations of parameters that are extremely sensitive to bead size. The surface mean radius of the silica-gel beads is only slightly larger than the average radius, so average radius can be used for estimating all pore parameters in this case with negligible difference.

The measured packing density values of the five types of silica-gel beads are very similar, with a value of 0.61. The packing density of spherical particles depends mainly on the packing mode and the size distribution of the particles [13]. The packing density of mono-sized spheres falls between 0.636 for random close packing [14] and 0.55 for random loose packing [13]. Although the five types of beads have different size ranges, they have very similar size distributions, as shown in Fig. 3, and almost identical loose packing conditions.

The coordination number (N_c) of the silica-gel beads is the average number of contact points each bead has with its nearest neighbors. The contact points for each bead were identified by counting the number of the deformed faces or dents for all the expanded and squeezed silica-gel beads subjected to the constrained heating. Fig. 4 shows the frequencies of silica-gel beads with different numbers of contact points. It is seen that most silica-gel beads have 5–9 deformed faces, giving an average number, i.e., coordination number, of 6.0. This measured coordination number is close to the reported range of 5.8–6.0 for randomly packed homogenous spheres [15,16]. The coordination number depends mainly on the packing mode and largely independent of particle size distribution [17], especially if the small-to-large size ratio is greater than 0.154 in the mixture of particles [13]. The silica-gel beads used in this paper falls within this situation.

3.2. Expansion ratio

The average densities and the average expanding ratios of the five types of silica-gel beads after the preheating treatment and the final heating process are listed in Table 1. Several observations can be made from the data. Firstly, the silica-gel beads experienced a large expansion during the preheating treatment. The expansion of the silica-gel beads during the final heating procedure is also significant. These expansions are irreversible, which is different from the thermal expansion of solid amorphous SiO_2, which is normally reversible and has a much lower linear expansion value. Secondly, the expansion ratio increases with preheating temperature. Comparing samples #2 and #4 shows that increasing the preheating temperature from 975 °C to 990 °C resulted in an increase in the expanding ratio from 0.20 to 0.26. Thirdly, smaller beads have a lower expansion ratio than larger beads. For example, at the same preheating temperature of 975 °C, increasing the raw bead radius from 0.25–0.36 mm (#4) to 0.36–0.50 mm (#3) increased the

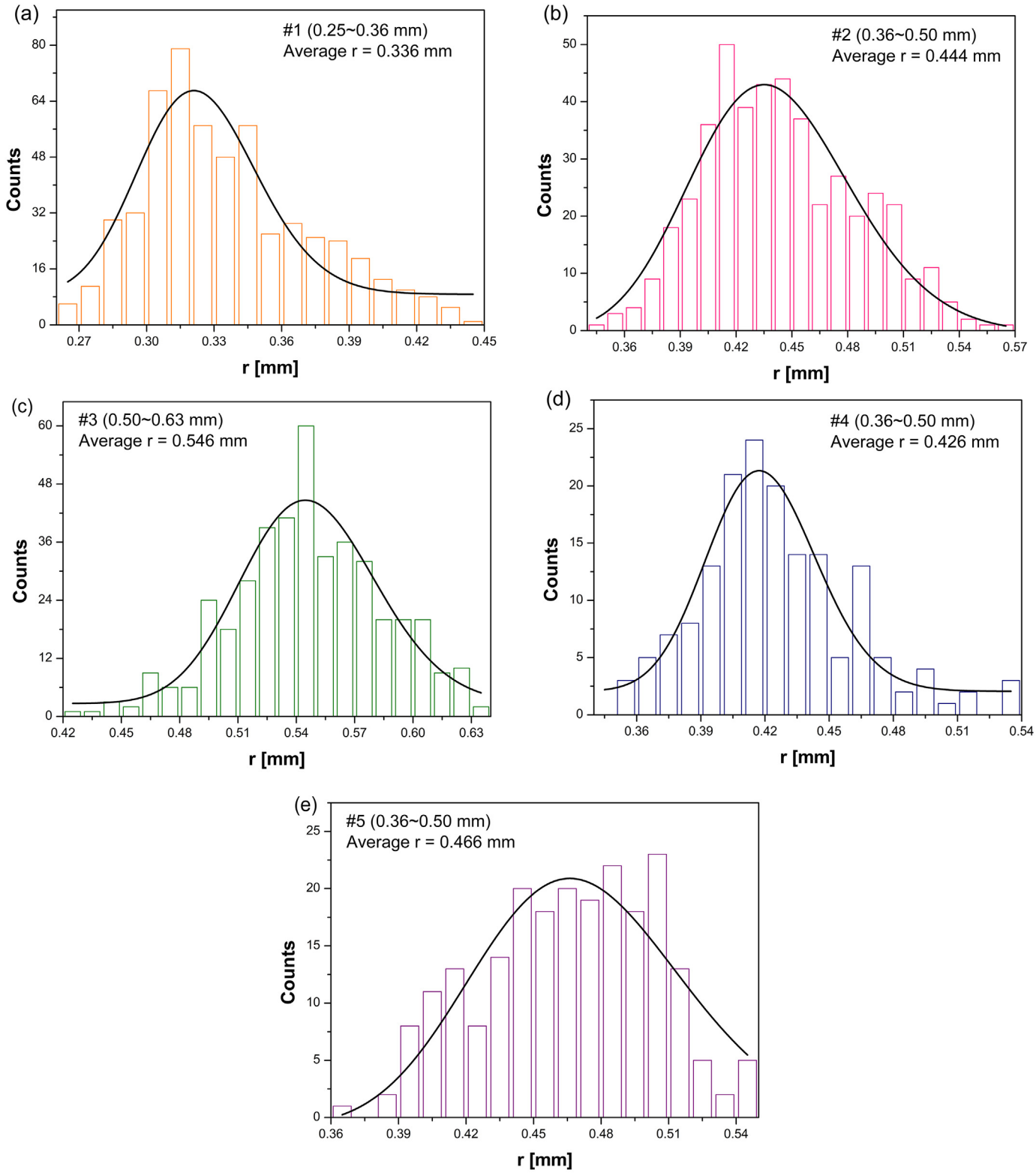

Fig. 3. Bead radius distributions of the five types of silica-gel beads.

expanding ratio from 0.20 to 0.30. Finally, the expansion ratio seems to increase with the density of the silica-gel beads. Sample #2 has the same bead size as sample #4 but a lower density (0.74 vs 0.82 g/cm^3) after preheating treatment. The final expansion ratio of #2 (0.024) is considerably lower than that of #4 (0.057).

3.3. Microstructure

Fig. 5 shows the cross-sections of silica-gel beads with a radius range of 1.0–1.25 mm before and after the preheating treatment. The raw silica-gel beads before preheating (Fig. 5a) has a nano-porous

Table 2
Comparison between experimental and calculated results of the pore structure parameters.

Silica-gel beads	Experimental results			Calculated results			Relative difference		
	P	R [mm]	S_v [cm^{-1}]	P	R [mm]	S_V [cm^{-1}]	δ_P (%)	δ_R (%)	δ_{Sv} (%)
#1	66.0%	0.362	53.5	65.0%	0.343	52.9	1.5	5.2	1.1
#2	66.0%	0.471	41.0	65.4%	0.455	40.0	0.9	3.4	2.4
#3	66.0%	0.580	32.5	65.9%	0.560	32.6	0.2	3.4	0.3
#4	71.0%	0.461	40.0	71.4%	0.450	40.1	0.6	2.4	0.3
#5	81.0%	0.532	33.6	83.0%	0.522	33.2	2.5	1.9	0.1

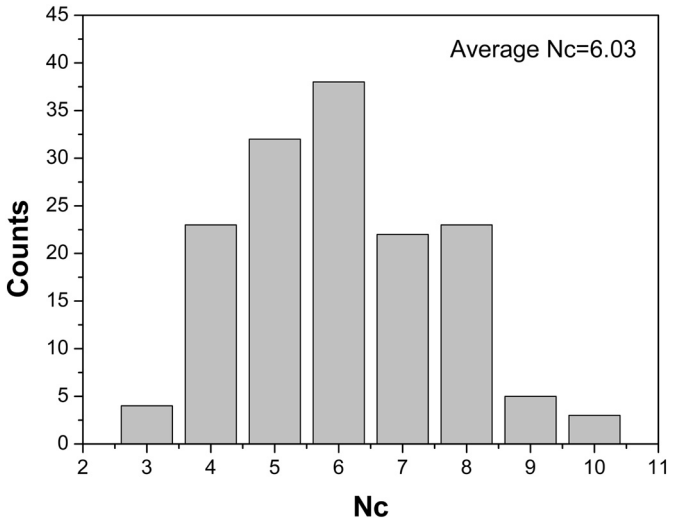

Fig. 4. Frequency of silica-gel beads with different numbers of contact points to their nearest neighbors.

microstructure (invisible at the low magnification, which was chosen for comparison purposes). Most of the silica-gel beads after expansion exhibit a double-layer microstructure with a nano-porous shell and a micro-porous core, as shown in Fig. 5b. The expansion of the silica-gel beads during preheating is apparently non-uniform, with the inner core expanding more than the shell. The inner core is composed of nearly spherical pores with overlapping pore walls.

Some of the silica-gel beads show a three-layer microstructure, as shown in Fig. 5c. It has a dense shell, a low-porosity core with small micro-pores, and a middle layer with large pores. This structure indicates that the expansion of the silica-gel beads starts from the middle layer and develops inwards. A double-layer structure is formed when the expansion propagates to the whole core region.

Occasionally, silica-gel beads with directional and damaged pores were observed (Fig. 5d). These directional and stream-lined pores span from the core center to the surface of the bead, accompanied by damaged shell (marked by arrows). This microstructure indicates that the high-pressure gas generated in the expansion of the silica-gel beads can break the pore walls, move towards the bead surface and break the shell before being released. The directional release of pressure leads to streamlined trails of elongated pores developing from the core to the damaged parts of the shell.

Fig. 6 shows the microstructural change of the silica-gel beads with a radius range of 0.36–0.50 mm during the final expansion stage when heated at 1100 °C for 20 min without constraint. It shows that the expansion process is a continuous development from the preheated structure, where the pores in the inner core become larger and the shell becomes thinner. The micro-pores in the core and the nano-pores in the shell both contribute to the final expansion.

3.4. Expansion mechanism

The irreversible deformation of the silica-gel beads and the spherical pores formed upon heating indicate that the driving force for the expansion is a gas coming from the silica-gel beads. Since the silica-gel beads consist of pure amorphous SiO_2 with a nano-porous structure, which can easily absorb water [18], it is reasonable to infer that the steam formed from the water confined in the silica-gel beads leads to the expansion.

Most water near the surface of the beads evaporates during the first step of preheating at 200 °C, forming a thin shell largely devoid of moisture. In the interior of the beads, the majority of the water is retained because water confined by the nano-sized pores is not easy to escape [18]. The poor thermal conductivity of amorphous SiO_2 leads to a relatively lower temperature in the interior, which may not produce a water vapor pressure high enough for the vapor to escape. When the beads are heated to 975–990 °C in the next step of the preheating treatment, the water remaining in the nano-pores vaporizes and produces a high pressure due to the hindrance of the solid pore wall. The high-pressure steam leads to pore wall deformation and expansion of the whole silica-gel beads. This is possible because even a tiny amount of water can generate a very high level of steam pressure when the temperature is above 600 °C [19].

The expansion of the silica-gel beads is not uniform. The initiation and propagation of expansion depend on the distribution of water content and temperature gradient within the bead. The surface shell of the bead is deficient in water after the first step of preheating and the new steam formed during the second step of preheating can escape more easily to the atmosphere. As a consequence, the shell does not expand much during the preheating treatment, although it has been heated up first. The expansion starts from a middle layer below the shell, because it has a combination of high water content and high temperature. There is a temperature gradient from the surface to the center of the bead due to its limited thermal conductivity. The expansion propagates inwards as temperature of the interior increases gradually during heating.

Silica-gel beads continue to expand during the final heating process, albeit to a less extent than during the preheating treatment. After preheating, a large proportion of the water contained in the beads is released, especially in the fully expanded regions. However, there is still water confined in the insufficiently expanded regions, especially the thin shell and the center region in those beads with a three-layer microstructure. When the beads are heated at a higher temperature, the remaining water vaporizes to generate a higher pressure, which produces an expansion.

The expansion processes during the preheating treatment and the final heating procedue are shown schematically in Fig. 7 and summarized as follows. The raw silica-gel beads contain numerous nano-pores which absorb and reserve water. The surface of the beads is dried during the first step of preheating at 200 °C, forming a shell deficient in moisture. During the preheating treatment at 975–990 °C, the water confined in the nanopores in the beads vaporizes to form high-pressure steam, which forces the pores to expand and deform. Expansion initiates from a middle layer below the shell and propagates inwards until the whole interior core is expanded. When the silica-gel beads are heated to a higher temperature during the final heating process, the residual water reserved in the shell and other non-fully-expanded regions vaporizes. The newly generated steam forces the pores to expand, resulting in a thinner shell and a larger core with larger pores.

The above mechanism explains well all the phenomena observed during the expansion process of the silica-gel beads upon heating. The

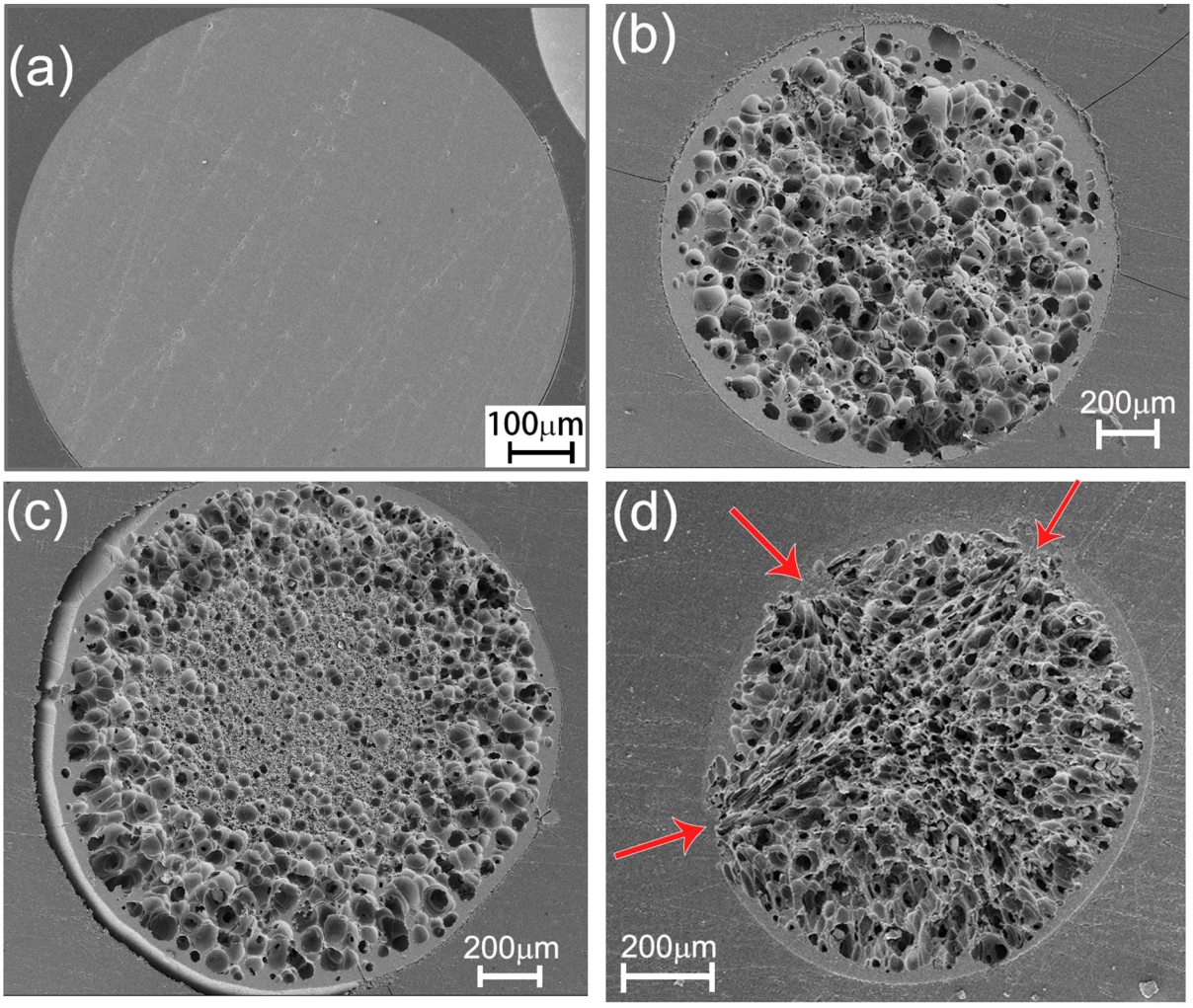

Fig. 5. Cross-sectional SEM images of silica-gel beads: (a) before preheating treatment; (b-d) after preheating treatment showing typical (b) two-layer, (c) three-layer and (d) directional/damaged pore structures.

driving force for the expansion is the vaporization of water confined in the nanopores in the silica-gel beads. The steam pressure is highly sensitive to temperature, so the expansion ratio is mainly determined by the heating temperature. Once the pore walls are stretched during expansion, the pores in the beads do not collapse during the subsequent cooling down, causing their irreversible deformation. Expansion starts in the middle layer and develops towards the bead center due to the existence of temperature gradient. If the expansion propagation terminates before reaching the center, a three-layer microstructure is formed. Most beads exhibit a two-layer structure because full expansion is achieved. Further expansion results in excessive steam pressure, which causes successive pore wall ruptures propagating radially towards the low pressure surface, especially at damaged parts of the surface. The shortest path of the chain ruptures is from the bead center to the bead surface, forming directional and streamlined ruptured pores as shown in Fig. 5d.

The mechanism can also explain the effects of bead size and density on the expansion ratio. Expansion ratio decreases with bead size because water contained in smaller beads evaporates and escapes more easily due to their higher specific surface areas and shorter distance of transport. The lower expansion ratio can be attributed to the lower water content in smaller beads. Preheated silica-gel beads with a higher density have more insufficiently expanded regions during the preheating treatment. These regions can sustain more expansion during the final heating process, leading to a higher expansion ratio.

4. Quantitative analysis of pore structure formed by silica-gel beads

4.1. Pore structure formation

In the silica-gel beads infiltration method, the silica-gel beads are placed underneath a master alloy before the alloy is melted and the melt is infiltrated into the interstices of the beads under pressure [3]. The weight of the mother alloy constrains the movement of the silica-gel beads during the heating process such that a well-bonded and stable space holder preform is formed. The metal fills the open space in the preform during melt infiltration and forms an intimate contact with the silica-gel beads. After solidification, the silica-gel beads are dissolved completely, resulting in a porous metal structure. The final porous structure is almost a replicate of the silica-gel bead preform.

The silica-gel beads undergo expansion during the heating process, before melt infiltration. While the beads maintain the same relative positions as the original packing, the beads are deformed and indented at the contact points due to the constrained expansion. Each touching point between the neighboring beads turns from a primarily point contact to a face contact. The originally spherical beads become polyhedrons as shown in Fig. 2.

The problem to predict the parametrical properties of the pore structure, therefore, becomes an analysis of the geometrical structure of the silica-gel beads preform after the final heating process but right before melt infiltration.

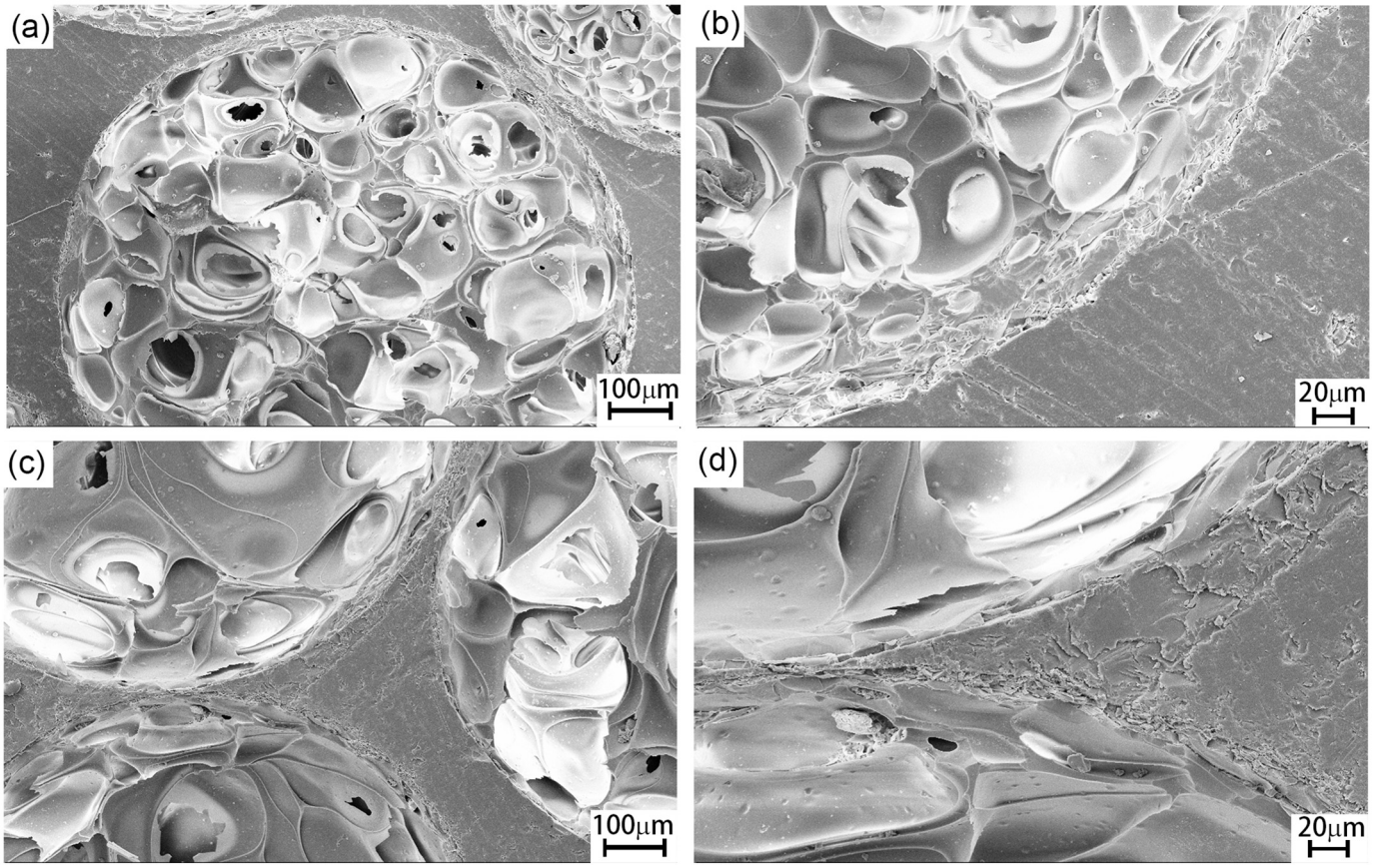

Fig. 6. Microstructure of the silica-gel beads: (a) and (b) after preheating treatment; (c) and (d) after final heating at 1100 °C for 20 min.

4.2. Pore size

Fig. 8 is a schematic diagram of the geometrical change of two adjacent silica-gel beads during the heating process. In practice, the bead size is not uniform and the expansion ratio of the beads is influenced by the bead size. However, it is impractical to determine the expansion ratios of all individual beads by experiment. A mean-field approach is sufficient to give an accurate representation. Let us assume that the beads are perfect spheres with an average radius of r and they are in direct contact with their neighbors at points before the heating. During the heating process, the beads expand to an average radius of R, by an average change of Δr. The touching points between the beads are deformed and/or crushed, and the contact points become circular contact faces of radius R_c, as shown in Fig. 8.

The pore size of the resultant foam is effectively the size of the silica-gel beads after expansion. The radius of the pores can therefore be expressed by:

$$R = r + \Delta r = r\left(1 + \frac{\Delta r}{r}\right) \quad (3).$$

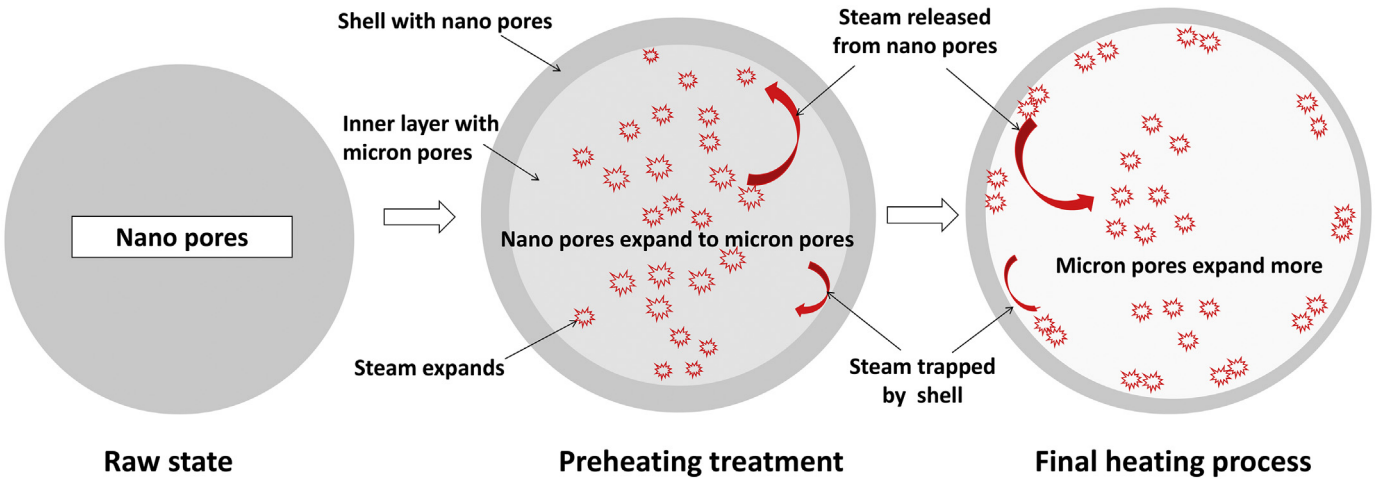

Fig. 7. Schematic diagram of the expansion process and microstructural change of the silica-gel beads during preheating and final heating processes.

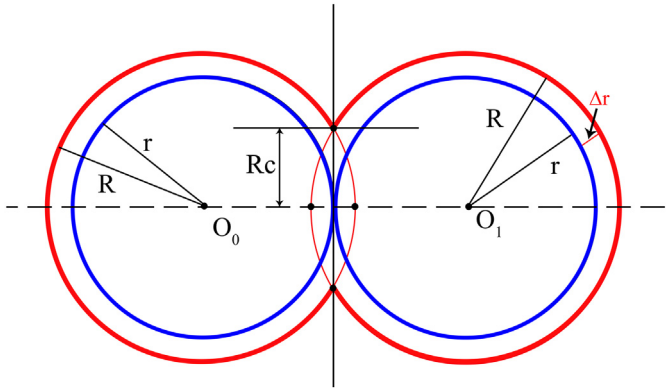

Fig. 8. Schematic diagram of the geometrical change of two adjacent silica-gel beads as they expand and deform.

4.3. Porosity

If the silica-gel beads were assumed not to expand during the final heating process, then the porosity of the resultant foam would be equal to the original packing density of the beads:

$$P_0 = K_{sp} \tag{4}$$

where P_0 is the porosity of the foam when the silica-gel beads do not expand and maintain their original shapes, and K_{sp} is the packing density of the silica-gel beads, which can be measured experimentally.

In the actual silica-gel bead infiltration method, however, the silica-gel beads do expand. The volume of the silica-gel beads increases due to the expansion, which results in an increase in the porosity in the end. The volume change is equal to the increase in the total volume of the beads under free expansion with a deduction of the volume loss at the contacts between the beads, or the total volume of all the spherical caps or dents, as illustrated in Fig. 8. Let us assume that the indented spherical caps are independent of one another, which is true when the expansion ratio is below 0.414 for a coordination number of about 6. Taking into account of the free expansion and the indented spherical caps between adjacent beads, the actual porosity of the foam can be calculated by:

$$P_1 = K_{sp}\frac{V_R - N_c V_{sc}}{V_r} = K_{sp}\frac{\frac{4}{3}\pi(r+\Delta r)^3 - \mathrm{N_c}\frac{\pi}{3}(3r+2\Delta r)\Delta r^2}{\frac{4}{3}\pi r^3}$$

$$= K_{sp}\left[1 + 3\frac{\Delta r}{r} + 3\left(1-\frac{N_c}{4}\right)\left(\frac{\Delta r}{r}\right)^2 + \left(1-\frac{N_c}{2}\right)\left(\frac{\Delta r}{r}\right)^3\right] \tag{5}$$

where V_r is the volume of the bead before expansion, V_R is the volume of the bead after expansion without indentation, V_{sc} is the volume of a spherical cap, N_c is the coordination number (the average number of contacts a bead has with its direct neighbors, which can be measured experimentally), r is the average radius of the bead before expansion, Δr is the average radius change of an expanded bead, and $\Delta r/r$ is defined as the average expansion ratio.

If the volume loss due to contact-point dents is ignored and only the free expansion is considered, the above equation can be simplified as:

$$P_2 = K_{sp}\left[1 + 3\frac{\Delta r}{r} + 3\left(\frac{\Delta r}{r}\right)^2 + \left(\frac{\Delta r}{r}\right)^3\right] \tag{6}$$

Eq. (6) can be further simplified, if higher-order items are ignored, as:

$$P_3 = K_{sp}\left(1 + 3\frac{\Delta r}{r}\right) \tag{7}$$

4.4. Specific surface area

The volumetric specific surface area, S_V, is the ratio of the total surface area of the pores to the volume of the porous metal sample. The surface area of the pores are equal to the part of the total surface area of the silica-gel beads that is in direct contact with the metal matrix. If the silica-gel beads do not expand, the specific surface area can be expressed by:

$$S_{V0} = K_{sp}\frac{S_r}{V_r} = \frac{3K_{sp}}{r} = \frac{3P_0}{r} \tag{8}$$

where S_{V0} is the specific surface area of the foam when the silica-gel beads do not expand and maintain their original shapes, and S_r is the surface area of a bead without expansion. Eq. (8) is in fact the expression for the volumetric specific surface area of closed-cell foam [20]. Since the beads do not expand, they are in point contacts with each other, effectively leading to a closed pore structure.

If the beads expand, free expansion would result in an increase in the surface area. Constrained expansion, however, leads to indentation between adjacent beads and thus a reduction of the surface in contact with the metal matrix, as illustrated in Fig. 8. This reduction is equal to the area of all the dents or the spherical caps. Taking into account of the free expansion and the indented spherical caps between adjacent beads, the specific surface area of the foam can be calculated by:

$$S_{V1} = K_{sp}\frac{S_R - N_c S_{sc}}{V_r} = K_{sp}\frac{4\pi(r+\Delta r)^2 - \mathrm{N_c}2\pi(r+\Delta r)\Delta r}{\frac{4}{3}\pi r^3}$$

$$= \frac{3K_{sp}}{r}\left[1 + \left(2-\frac{N_c}{2}\right)\frac{\Delta r}{r} + \left(1-\frac{N_c}{2}\right)\left(\frac{\Delta r}{r}\right)^2\right] \tag{9}$$

where S_R is the surface area of the bead after expansion without indentation, and S_{sc} is the surface area of a spherical cap.

If the surface loss due to contact-point dents is ignored and only the free expansion is considered, the above equation can be simplified as:

$$S_{V2} = \frac{3K_{sp}}{r}\left(1 + \frac{\Delta r}{r}\right)^2 \tag{10}$$

4.5. Influence of expansion ratio on porosity and specific surface area

It is obvious that pore size of the foam increases linearly with expansion ratio of the silica-gel beads, as shown in Eq. (3), since the increment of pore size is the direct effect of the expansion of the beads.

The influence of expansion ratio on porosity, however, is more complex. The expansion of the silica-gel beads leads to an increment of pore volume, whereas the indentation between adjacent beads leads to a decrement of pore volume. The predictions of porosity as a function of expansion ratio based on Eqs. (5), (6) and (7), assuming a packing density of beads $K_{sp} = 0.61$ and a coordination number $N_c = 6.0$, are shown in Fig. 9a. P1, which is the actual porosity taking into account expansion and indentation of beads, is shown to increase with the expansion ratio. An expansion ratio of 0.1 can increase the porosity from 0.6 to 0.75, which is apparently significant.

Fig. 9a also shows that P2, which is an approximate porosity taking into account the expansion but ignoring indentation, is very close to P1 when the expansion ratio is below 0.06 but considerably different from P1 when the expansion ratio is above 0.08. This means that the

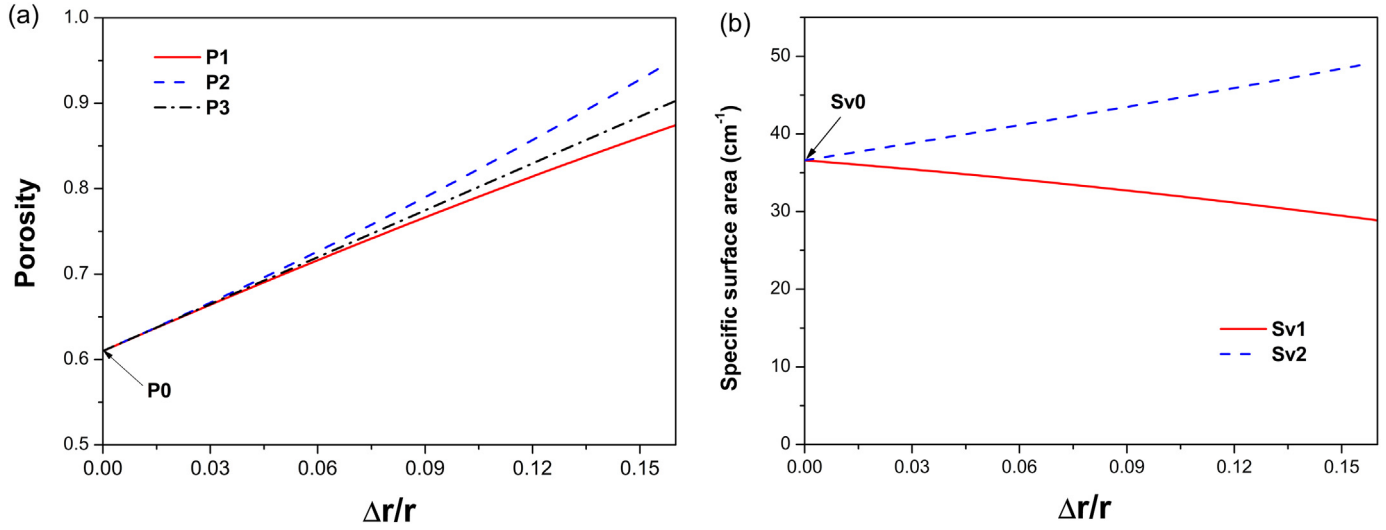

Fig. 9. Relationship of (a) porosity and (b) specific surface area with expansion ratio. P1, P2 and P3 denote porosity predictions based on Eqs. (5)–(7). Sv1 and Sv2 denote specific surface area predictions based on Eqs. (9) and (10).

effect of bead indentation can be neglected at low expansion ratios but it has to be considered at high expansion ratios. P3, which is an approximate porosity predicted from the much simplified Eq. (7), is always below P2 and slightly above P1, with the relative difference between P3 and P1 less than 2% for the expansion ratio in a wide range of 0–0.12. Therefore, Eq. (7) is a good approximation for porosity estimation of the foams manufactured by the silica-gel bead infiltration method.

The influence of expansion ratio on specific surface area, predicted by Eqs. (9) and (10), assuming a packing density $K_{sp} = 0.61$ and a coordination number $N_c = 6.0$ and bead radius $r = 0.5$ mm, can be seen in Fig. 9b. The specific surface area, S_{V1}, decreases nearly linearly with expansion ratio. An expansion ratio of 0.1 can result in a significant decrease of specific surface area from 35 cm^{-1} to 30 cm^{-1}. It indicates that surface area reduction due to the indentation between adjacent beads during expansion is a significant factor and cannot be ignored. Ignoring the indentation and considering the expansion alone leads to an increasing specific surface area, S_{V2}, with expansion ratio. This shows a completely wrong trend. Therefore, the simplified equation, Eq. (10), should not be used for estimating specific surface area.

The porosity and specific surface area of the foam are proportional to the packing density of the silica-gel beads, as shown in Eqs. (5) and (9), respectively. The coordination number also affects porosity and specific surface area. However, packing denisty and coordination number do not change much in the silica-gel bead infiltration method. It is reasonable to take packing density as $K_{sp} = 0.61$ and coordination number as $N_c = 6.0$ in all estimations.

4.6. Comparison with experimental results

The measured values for pore size (R), porosity (P) and specific surface area (S_V) of Cu-Al-Mn foams [3] manufactured by the silica-gel bead infiltration method using the five types of silica-gel beads (#1 ~ #5) are listed in Table 2. Their counterpart calculated values obtained by Eqs. (3), (5) and (9), respectively, are also listed in Table 2 for comparison. The measured packing density ($K_{sp} = 0.61$) and average coordination number ($N_c = 6.0$) values are used in all calculations. The values of average bead radius ($\bar{r}$), surface mean radius ($\bar{r}_s$) and expansion ratio during final heating($\Delta r/r$) used for the calculations are listed in Table 1. Average bead radius is used in calculating pore size and porosity and surface mean radius is used in calculating specific surface area.

Table 2 shows that the differences between the calculated and experimental results for all the pore structural parameters are relatively small. The calculated porosity values almost coincide with the experimental results, with a small difference of 0.2% ~ 1.5%. The difference between the calculated and experimental pore size is 1.9% ~ 5.2%, which is small considering the wide bead size distributions. The difference in specific surface area is also small, about 0.1% ~ 2.4%. This demonstrates that the geometrical model developed in this paper is reliable and the equations used for estimating porosity, pore size and specific surface area as a function of expansion ratio are reasonably accurate.

5. Conclusions

1) Expansion ratios of silica-gel beads during the preheating and final heating processes were measured. The irreversible and non-uniform expansion of silica-gel beads was caused by high-pressure steam generated from water confined in the nano-pores of the silica-gel beads. This mechanism can explain well all the phenomena observed during the expansion process.

2) The packing density of the silica-gel beads was measured to be 0.61. During the heating process, the silica-gel beads underwent expansion and, when constrained, the contact points between the adjacent beads were indented and formed deformed faces. The average number of dents per bead, or coordination number, was measured to be 6.0.

3) A geometrical model was developed to calculate the pore size, porosity and specific surface area of metal foams manufactured from the silica-gel bead preform, as a function of expansion ratio. The influence of the indented spherical caps on the model calculations was discussed. While the dents can be ignored for calculating the porosity at low expansion ratios, it has to be taken into account for calculating porosity at high expansion ratios and for calculating specific surface area.

4) The differences between the calculated and experimental values for pore size, porosity and specific area are relatively small (0.1% ~ 5.2%), demonstrating that the geometrical model is reliable and reasonably accurate.

Declaration of Competing Interest

The authors declare that they have no known competing financial interests or personal relationships that could have appeared to influence the work reported in this paper.

Acknowledgments

The authors acknowledge the financial support from the Natural Science Foundation of Guangdong Province [2016A030311012], and the China Scholarship Council [201706150040].

References

[1] G. Bertolino, P.A. Larochette, E.M. Castrodeza, et al., Mechanical properties of martensitic Cu–Zn–Al foams in the pseudoelastic regime, Mater. Lett. 64 (13) (2010) 1448–1450.
[2] H. Li, B. Yuan, Y. Gao, Y.Y. Zhao, Effect of oligocrystallinity on damping and pseudoelasticity of oligocrystalline Cu-Al-Mn shape memory foams, J. Alloys Compd. 773 (2019) 940–949.
[3] H. Li, B. Yuan, Y. Gao, Achieving high oligocrystalline degree via strut architecture tailoring to increase the damping and mechanical properties of spherical porous CuAlMn SMAs, J. Alloys Compd. 767 (2018) 690–702.
[4] Q.Z. Wang, F. Han, J. Wu, et al., Damping behavior of porous CuAlMn shape memory alloy, Mater. Lett. 61 (s 11–12) (2007) 2598–2600.
[5] J. Banhart, Manufacture, characterisation and application of cellular metals and metal foams, Prog. Mater. Sci. 46 (6) (2001) 559–632.
[6] M.W.D. Van der Burg, V. Shulmeister, E. Van der Geissen, et al., On the linear elastic properties of regular and random open-cell foam models, J. Cell. Plast. 33 (1) (1997) 31–54.
[7] S. Gong, Z. Li, G. Xu, et al., Fabrication, microstructure and property of cellular CuAlMn shape memory alloys produced by sintering–evaporation process, J. Alloys Compd. 509 (2011) 2924–2928.
[8] Q. Wang, C. Cui, Q. Wang, et al., Fabrication of a porous CuAlMn shape memory alloy by the sintering–dissolution process, Mater. Lett. 65 (2011) 2735–2738.
[9] B. Yuan, P. Zheng, Y. Gao, et al., Effect of directional solidification and porosity upon the superelasticity of Cu–Al–Ni shape-memory alloys, Mater. Design 80 (2015) 28–35.
[10] E.M. Castrodeza, C. Mapelli, M. Vedani, et al., Processing of shape memory CuZnAl open-cell foam by molten metal infiltration, J. Mater. Eng. Perform. 18 (2009) 484–489.
[11] H. Li, B. Yuan, Y. Gao, Processing of CuAlMn shape memory foams with open spherical pores by silica-gel beads infiltration method, Metall. Mater. Trans. B Process Metall. Mater. Process. Sci. 47 (5) (2016) 3168–3177.
[12] Q.D. Tan, Forest Statistical Analysis, Ericsson Supplies Agency, 1953.
[13] G.C. Barker, A. Mehta, Vibrated powders: structure, correlations, and dynamics, Phys. Rev. A 45 (6) (1992) 3435–3446.
[14] G.D. Scott, D.M. Kilgour, The density of random close packing of spheres, J. Phys. D. Appl. Phys. 2 (6) (1969) 863–866.
[15] J.S. Goodling, M.S. Khader, Co-ordination number distribution of spherical particles in a packed cylindrical bed, Powder Technol. 44 (1) (1985) 53–55.
[16] A. Yang, C.T. Miller, L.D. Turcoliver, Simulation of correlated and uncorrelated packing of random size spheres, Phys. Rev. E Stat. Phys. Plasmas Fluids Relat. Interdisc. Topics 53 (2) (1996) 1516–1524.
[17] D. Pinson, R.P. Zou, A.B. Yu, et al., Coordination number of binary mixtures of spheres, J. Phys. D. Appl. Phys. 20 (31) (1998) 457–462.
[18] M. Oguni, S. Maruyama, K. Wakabayashi, et al., Glass transitions of ordinary and heavy water within silica-gel nanopores, Chem. Asian J. 2 (4) (2007) 514–520.
[19] D. Wang, J. Tan, X. Zhang, et al., High pressure steam–water two-phase flow measurements by flow division and separation method, Exp. Thermal Fluid Sci. 44 (2013) 468–474.
[20] H.E. Deping, Y.U. Xinquang, Effect of pore structure parameters on the non~linear damping capacity of new type foamed aluminium with open pore structure, Chin. J. Mater. Res. 11 (1) (1997) 101–103.